Advances in Mathematical Sciences and Applications
Vol. 30, No. 1 (2021), pp. 175–189

GAKKOTOSHO
TOKYO JAPAN

DEVELOPMENT OF A HIGH-PRECISION NUMERICAL METHOD FOR INTEGRATION OVER ONE PERIOD OF PERIODIC FUNCTIONS WITH A SHARP PEAK

Hirokazu Ito
Graduate School of Science and Engineering, Doshisha University,
1-3 Tatara Miyakodani, Kyotanabe, Kyoto, 610-0394, Japan
(E-mail: ctwd0903@mail4.doshisha.ac.jp)

Hitoshi Imai
Faculty of Science and Engineering, Doshisha University,
1-3 Tatara Miyakodani, Kyotanabe, Kyoto, 610-0394, Japan
(E-mail: himai@mail.doshisha.ac.jp)

and

Takuya Ooura
Research Institute for Mathematical Sciences, Kyoto University,
Kitashirakawaoiwakecho, Sakyoku, Kyoto, 606-8502, Japan
(E-mail: ooura@kurims.kyoto-u.ac.jp)

Abstract. In the paper, a high-precision numerical integration method PAT(peak adjustment transform) is proposed. PAT requires a discretization method with non-equidistant collocation points. PAT is valid for the integration over one period of periodic functions with a sharp peak which makes high-precision numerical integration difficult. Numerical computations are carrid in multiple precision. Numerical results are very satisfactory in accuracy.

Communicated by Editors; Received 5 April, 2021
This work was supported by JSPS KAKENHI Grant Numbers 18K03436 and 16H02155.
AMS Subject Classification: 34G20, 34K28, 65L05.
Keywords: numerical integration, spectral method, peak, accuracy, multiple-precision.

1 Introduction

X-ray CT(computed tomography) or MRI(magnetic resonance imaging) are famous technologies for non-destructive inspection of the human body. However, these technologies have problems such as exposure to x-rays or strict restrictions on magnetic materials. Recenently, the near-infrared(NIR) light CT has been attracting attention. This is because it is free from such problems and it can be inexpensive. NIR light passes through the human tissue with diffusion and radiation. In the two-dimensional stationary case, this NIR light propagation in the tissue is modeled as the following boundary value problem(BVP) with a radiation transport equation(RTE) [5–8, 12].

$$-\boldsymbol{\xi} \cdot \nabla_{\boldsymbol{x}} I(\boldsymbol{x}, \boldsymbol{\xi}) - (\mu_s + \mu_a) I(\boldsymbol{x}, \boldsymbol{\xi}) + \mu_s \int_{S^1} p(\boldsymbol{x}; \boldsymbol{\xi}, \boldsymbol{\xi'}) I(\boldsymbol{x}, \boldsymbol{\xi'}) \, d\sigma_{\xi'} = 0 \text{ in X}, \tag{1}$$

$$I(\boldsymbol{x}, \boldsymbol{\xi}) = I_1(\boldsymbol{x}, \boldsymbol{\xi}) \text{ on } \Gamma_-. \tag{2}$$

Here, $\boldsymbol{x} = (x,\ y)$ is the spatial position in $\Omega \subset \mathbb{R}^2$, $\nabla_{\boldsymbol{x}} = (\frac{\partial}{\partial x}, \frac{\partial}{\partial y})$, $\boldsymbol{\xi}$ is the unit vector which denotes the direction of flight, $X = \Omega \times S^1$, $I_1(\boldsymbol{x}, \boldsymbol{\xi})$ is a given function. For a outward unit vector $\boldsymbol{n(x)}$ on $\partial\Omega$, $\Gamma_- = \{(\boldsymbol{x},\ \boldsymbol{\xi}) : \boldsymbol{x} \in \partial\Omega, \boldsymbol{n(x)} \cdot \boldsymbol{\xi} < 0\}$. $I(\boldsymbol{x}, \boldsymbol{\xi})$ denotes the energy radiance. μ_a and μ_s are the absorption and scattering coefficients, respectively. $p(\boldsymbol{x}; \boldsymbol{\xi}, \boldsymbol{\xi'})$ is the scattering phase function that describes the probability that a photon with the direction $\boldsymbol{\xi'}$ is scattered to the direction $\boldsymbol{\xi}$ during a scattering event. $p(\boldsymbol{x}; \boldsymbol{\xi}, \boldsymbol{\xi'})$ satisfies the following conditions;

$$p(\boldsymbol{x}; \boldsymbol{\xi}, \boldsymbol{\xi'}) \geq 0, \quad \int_{S^1} p(\boldsymbol{x}; \boldsymbol{\xi}, \boldsymbol{\xi'}) \, d\sigma_{\boldsymbol{\xi'}} = 1.$$

Since it is difficult to solve the above boundary value problem exactly, we have to rely on numerical computations. Practically, the above boundary value problem is considered in the three-dimensional space. Since there is an integral term, numerical computations are performed in the five-dimensional space. In such huge-scale numerical computations, saving computational time is crucial. Thus, low-order approximations as finite difference methods are used [5–7].

On the other hand, we have been involved in high-precision numerical computations and their applications [3, 9, 11, 13]. Although we have developed numerical methods for high-precision numerical computations, it is not easy to solve the above boundary value problem numerically and accurately. This is bacause that even if the solution $I(\boldsymbol{x}, \boldsymbol{\xi})$ is smooth and gentle, the integrand may become singular due to the integral kernel $p(\boldsymbol{x}; \boldsymbol{\xi}, \boldsymbol{\xi'})$. In the paper, we consider high-precision numerical computation of the following definite integral;

$$F(\theta) \equiv \int_0^{2\pi} p(\phi - \theta) I(\phi) \, d\phi, \tag{3}$$

where functions p and I are periodic with period 2π, $p(\phi) \geq 0$, $\displaystyle\int_0^{2\pi} p(\phi) \, d\phi = 1$. We consider two kinds of periodic integral kernels with period 2π, i.e. the Poisson kernel

p_o [5] and the power function kernel p_{ow} as follows;

$$p_o(\phi-\theta) \equiv \frac{1}{2\pi}\frac{1-g^2}{1-2g\cos(\phi-\theta)+g^2}, \qquad 0 \le \phi < 2\pi, \tag{4}$$

$$p_{ow}(\phi-\theta) \equiv \begin{cases} \dfrac{m+1}{2\pi}\left(\dfrac{\phi+2\pi-\theta}{\pi}-1\right)^m, & 0 \le \phi \le \theta, \\[2ex] \dfrac{m+1}{2\pi}\left(\dfrac{\phi-\theta}{\pi}-1\right)^m, & \theta < \phi < 2\pi, \end{cases} \tag{5}$$

where $g\,(0 < g < 1)$ and $\theta\,(0 \le \theta < 2\pi)$ are constant, $m_{half} \in \mathbb{Z}_+$, $m = 2m_{half}$. As is shown in Figures 1 and 2, both kernels have a peak at $\phi = \theta$ and the sharpness of the peak depends on g and m.

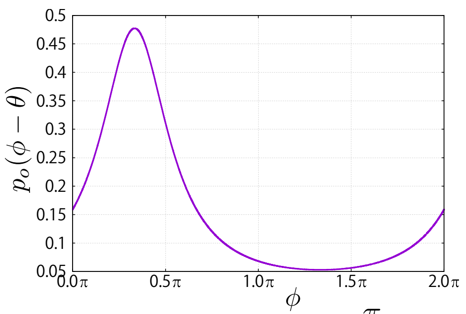

(1) $g = 0.5$, $\theta = \dfrac{\pi}{3}$

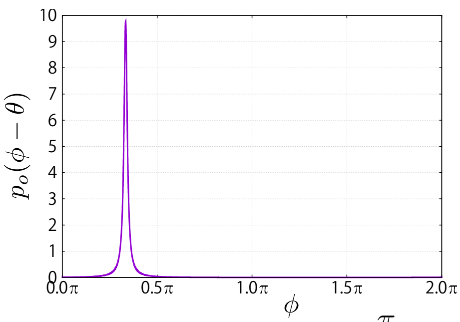

(2) $g = 0.968$, $\theta = \dfrac{\pi}{3}$

Figure 1: Profile of the Poisson kernel $p_o(\phi-\theta)$.

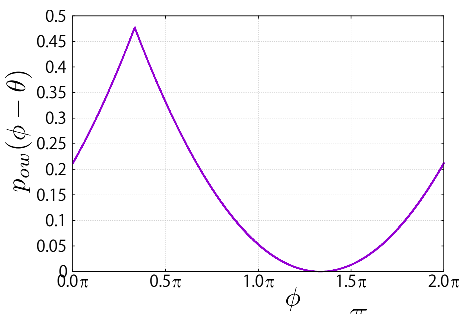

(1) $m = 2$, $\theta = \dfrac{\pi}{3}$

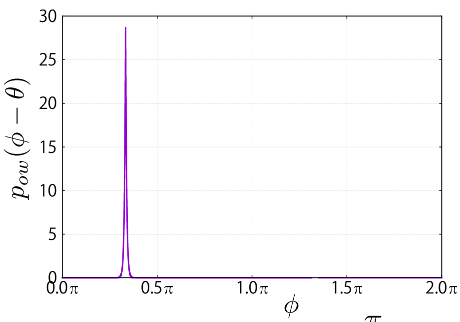

(2) $m = 180$, $\theta = \dfrac{\pi}{3}$

Figure 2: Profile of the power function kernel $p_{ow}(\phi-\theta)$.

Considering applications to a BVP with RTE, we set $I(\phi) = 1,\ \cos h\phi,\ \sin h\phi,\quad h \in \mathbb{Z}_+$. Figure 3 shows an example that the integrand in (3) becomes almost singular for smooth and gentle $I(\phi)$. This shows the difficulty of high-precision numerical computations to (3). To overcome to this difficulty, in the paper, we present a numerical method called PAT(peak adjustment transform).

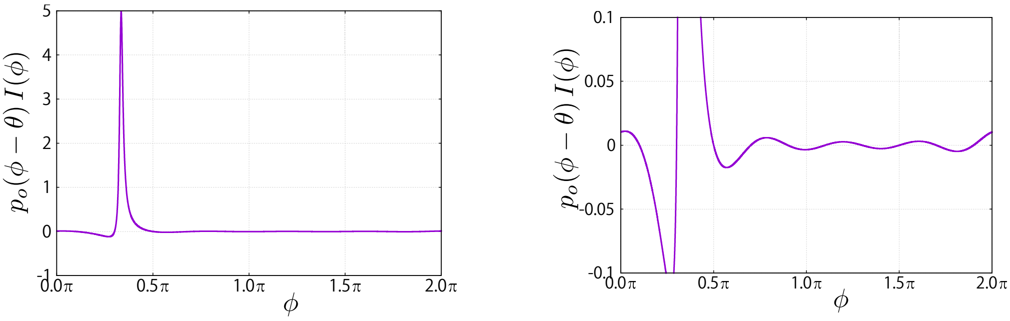

(1) $I(\phi) = \cos 5\phi$. (2) Vertically enlarged view.

Figure 3: Profile of integrand $p_o(\phi - \theta)\, I(\phi)$ $\left(g = 0.968, \theta = \dfrac{\pi}{3}\right)$.

2 Exact value of the definite integral

We need to obtain the exact value of $F(\theta)$ in (3) to evaluate the validity of our numerical method.

The exact value for the Poisson kernel can be found using the residue theorem. The result is as follows;

$$F(\theta) = \begin{cases} \displaystyle\int_0^{2\pi} p_o(\phi-\theta)\cos h\phi\, d\phi = g^h \cos h\theta, \\ \displaystyle\int_0^{2\pi} p_o(\phi-\theta)\sin h\phi\, d\phi = g^h \sin h\theta. \end{cases} \tag{6}$$

In the case of the power function kernel, we need a little complicated calculation. We set

$$P_m(\theta) \equiv \int_0^{2\pi} p_{ow}(\phi-\theta)\cos h\phi\, d\phi, \qquad Q_m(\theta) \equiv \int_0^{2\pi} p_{ow}(\phi-\theta)\sin h\phi\, d\phi.$$

When m = 2, the exact values can be obtained directly and easily as follows:

$$P_2(\theta) = \frac{6}{\pi^2 h^2}\cos h\theta, \qquad Q_2(\theta) = \frac{6}{\pi^2 h^2}\sin h\theta.$$

For general m it should be noted that m is even and the functions p_{ow} and I are periodic. We consider

$$P_m(\theta) + i\,Q_m(\theta) = \int_0^{2\pi} \frac{m+1}{2\pi}\left(\frac{\psi}{\pi} - 1\right)^m (\cos h(\psi+\theta) + i\,\sin h(\psi+\theta))\;d\psi,$$
$$= \mathrm{e}^{ih\theta}\int_0^{2\pi} \frac{m+1}{2\pi}\left(\frac{\psi}{\pi} - 1\right)^m \mathrm{e}^{ih\psi}\,d\psi.$$

Here,

$$R_m \equiv \int_0^{2\pi} \frac{m+1}{2\pi}\left(\frac{\psi}{\pi} - 1\right)^m \mathrm{e}^{ih\psi}\,d\psi = -\frac{(m+1)m}{i2h\pi^{m+1}}\int_0^{2\pi} (\psi-\pi)^{m-1}\,\mathrm{e}^{ih\psi}\,d\psi,$$
$$= \frac{(m+1)m}{h^2\pi^2} - \frac{(m+1)m}{h^2\pi^2}S_{m-2},$$
$$= \frac{(m+1)m}{h^2\pi^2} - \frac{(m+1)m(m-1)(m-2)}{h^4\pi^4}$$
$$+ (-1)^2\frac{1}{h^6\pi^6}(m+1)m(m-1)(m-2)(m-3)(m-4)$$
$$+ \cdots + (-1)^{\frac{m-2}{2}}\frac{1}{h^{m-2}\pi^{m-2}}(m+1)m\cdots 5\cdot 4\cdot R_2.$$

Since $R_2 = P_2(0) + i\,Q_2(0) = \dfrac{6}{h^2\pi^2}$, $\qquad R_m = \displaystyle\sum_{l=1}^{m_{half}}\left(\frac{(-1)^{l-1}}{h^{2l}\pi^{2l}}\prod_{j=m_{half}}^{m_{half}-l+1}(2j+1)2j\right).$

This shows that R_m is a real number, and we get

$$F(\theta) = \begin{cases} \displaystyle\int_0^{2\pi} p_{ow}(\phi-\theta)\cos h\phi\,d\phi = P_m(\theta) = R_m\cos h\theta, \\ \displaystyle\int_0^{2\pi} p_{ow}(\phi-\theta)\sin h\phi\,d\phi = Q_m(\theta) = R_m\sin h\theta. \end{cases} \tag{7}$$

3 Direct numrical integrations and remarks

It is known that spectral methods are superior in accuracy among discretization methods [1,2]. In particular, the spectral collocation method(SCM) is highly applicable. Hereafter, SCM for Fourier series, i.e. the discrete Fourier transform, is written as Fourier-SCM, and SCM for Chebyshev polynomials is written as Chebyshev-SCM. Our numerical integration for a given function f is performed as follows;

$$\int_0^{2\pi} f(\phi)\,d\phi \fallingdotseq \int_0^{2\pi} f_d(\phi)\,d\phi,$$

where we make an approximate function $f_d(\phi)$ for $f(\phi)$ by SCM [10]. As direct numerical integrations, we apply Fourier-SCM and Chebyshev-SCM to make $f_d(\phi)$.

3.1 Fourier-SCM

Let $K_{\max}$ be an even number. In Fourier-SCM, collocation points are given as $\phi_{k_f} = \dfrac{2k_f\pi}{K_{\max}}, \quad k_f = 1, 2, \cdots, K_{\max}$, and

$$f_d(\phi) = \frac{1}{2}\tilde{a}_0 + \sum_{k=1}^{K_{\max}/2-1} \left(\tilde{a}_k \cos k\phi + \tilde{b}_k \sin k\phi\right) + \frac{1}{2}\tilde{a}_{K_{\max}/2} \cos\left(\frac{K_{\max}}{2}\phi\right), \quad 0 \le \phi \le 2\pi,$$

$$\tilde{a}_k = \frac{2}{K_{\max}} \sum_{k_f=1}^{K_{\max}} f_{k_f} \cos k\phi_{k_f}, \quad \tilde{b}_k = \frac{2}{K_{\max}} \sum_{k_f=1}^{K_{\max}} f_{k_f} \sin k\phi_{k_f}, \quad f_{k_f} = f_d(\phi_{k_f}).$$

When $f_{k_f} = f(\phi_{k_f})$, $f_d(\phi)$ becomes an approximate function for $f(\phi)$. Thus, numerical integration is given as follows:

$$\int_0^{2\pi} f(\phi)\, d\phi \fallingdotseq \int_0^{2\pi} f_d(\phi)\, d\phi = \frac{2\pi}{K_{\max}} \sum_{k_f=1}^{K_{\max}} f_{k_f}, \quad f_{k_f} = f(\phi_{k_f}). \tag{8}$$

3.2 Chebyshev-SCM

Let N be an integer. We consider Chebyshev Gauss-Lobatto(CGL) collocation points $\bar{x}_j = \cos\dfrac{j\pi}{N}, \quad j = 0, 1, \cdots, N$. Hereafter, Chebyshev-SCM with CGL collocation points is written as CGL-SCM. Then, for a polynomial of degree N $\tilde{U}_N(x)$,

$$\tilde{U}_N(x) = \sum_{k=0}^{N} \bar{a}_k T_k(x), \quad -1 \le x \le 1, \qquad \bar{a}_k = \frac{2}{N\bar{c}_k} \sum_{j=0}^{N} \frac{1}{\bar{c}_j} T_k(\bar{x}_j)\tilde{U}_j, \quad \tilde{U}_j = \tilde{U}_N(\bar{x}_j),$$

where

$$T_k(x) = \cos(k \arccos x), \quad k = 0, \cdots, N, \qquad \bar{c}_j = \begin{cases} 2, & j = 0, N, \\ 1, & j = 1, \cdots, N-1. \end{cases}$$

When $\tilde{U}_j = U(\bar{x}_j)$, $\tilde{U}_N(x)$ becomes an approximate function for $U(x)$. From this, we applied a direct numerical integration method to an inverse problem [10]. The method is as follows. For an integer $K_{\max}$, an approximate function $f_d(\phi)$ for $f(\phi)$ is generated as follows;

$$
f(\phi) \fallingdotseq f_d(\phi) = \sum_{k_0=0}^{K_{\max}} f_{k_0} T_{k_0}(z), \quad z = \frac{\phi}{\pi} - 1, \quad f_{k_0} = \frac{2}{c_{k_0} K_{\max}} \sum_{k_1=0}^{K_{\max}} \frac{1}{c_{k_1}} f(\phi_{k_1}) T_{k_0}\left(z_{k_1}\right),
$$

$$
\phi_{k_1} = \pi\left(z_{k_1}+1\right), \qquad z_{k_1} = \cos\left(\frac{k_1 \pi}{K_{\max}}\right), \quad c_* = \begin{cases} 2, & * = 0, K_{\max}, \\ 1, & \text{otherwise}, \end{cases} \qquad * = k_0,\, k_1.
$$

Thus, numerical integration is given as follows;

$$
\int_0^{2\pi} f(\phi)\, d\phi \fallingdotseq \int_0^{2\pi} f_d(\phi)\, d\phi = \int_{-1}^{1} \pi f_d(\pi(z+1))\, dz = \pi \sum_{\substack{k_0=0 \\ k_0 \neq 1}}^{K_{\max}} f_{k_0} \frac{1+(-1)^{k_0}}{1-k_0^2}. \tag{9}
$$

3.3 Remarks for direct numerical integrations

We show some remarks for above direct numerical integrations by numerical results. Numerical computations are performed in 100 digits using exflib [4]. Here, we set $I(\phi) = 1$, i.e. $F(\theta) = 1$.

Numerical results for the Poisson kernel are shown in Figure 4. When the integrand is gentle ($g = 0.5$), accuracy is very nice and Fourier-SCM is a little more accurate than Chebyshev-SCM. When the integrand has a sharp peak ($g = 0.968$), accuracy is poor except when $\theta = 0$ in Chebyshev-SCM.

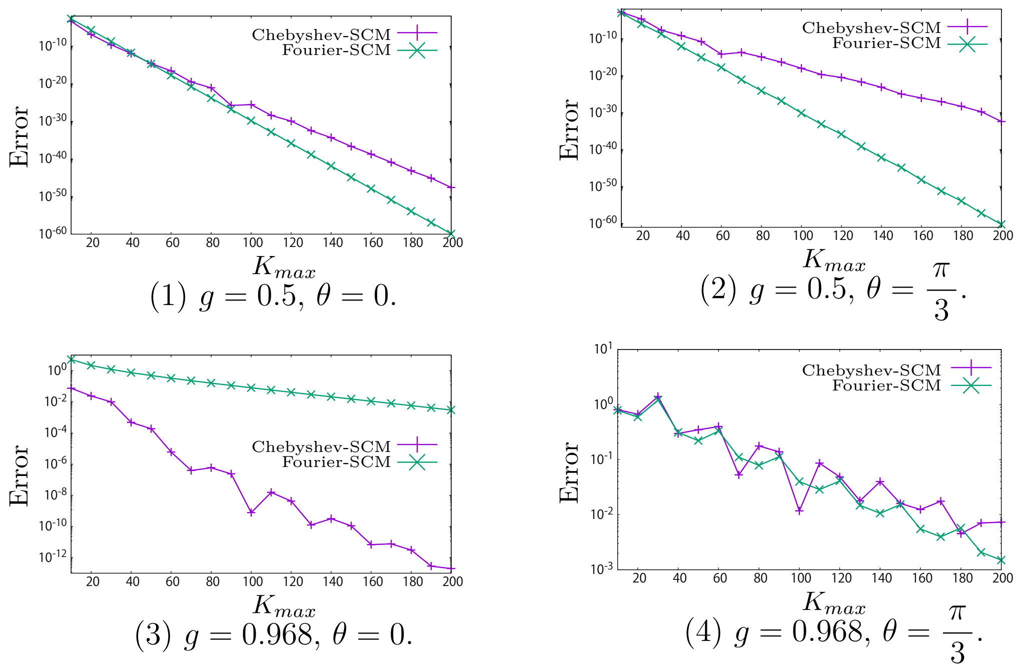

(1) $g = 0.5$, $\theta = 0$.

(2) $g = 0.5$, $\theta = \dfrac{\pi}{3}$.

(3) $g = 0.968$, $\theta = 0$.

(4) $g = 0.968$, $\theta = \dfrac{\pi}{3}$.

Figure 4: Error for $F(\theta)$ (Poisson kernel, $I(\phi) = 1$).

Numerical results for the power function kernel are shown in Figure 5. Accuracy of Fourier-SCM is very poor because the integrand cannot be differentiated at the peak. When $N \geq m$ there is no truncation error as is shown in Figures 5(1) and 5(3). When $\theta \neq 0$, accuracy of both SCM is almost same.

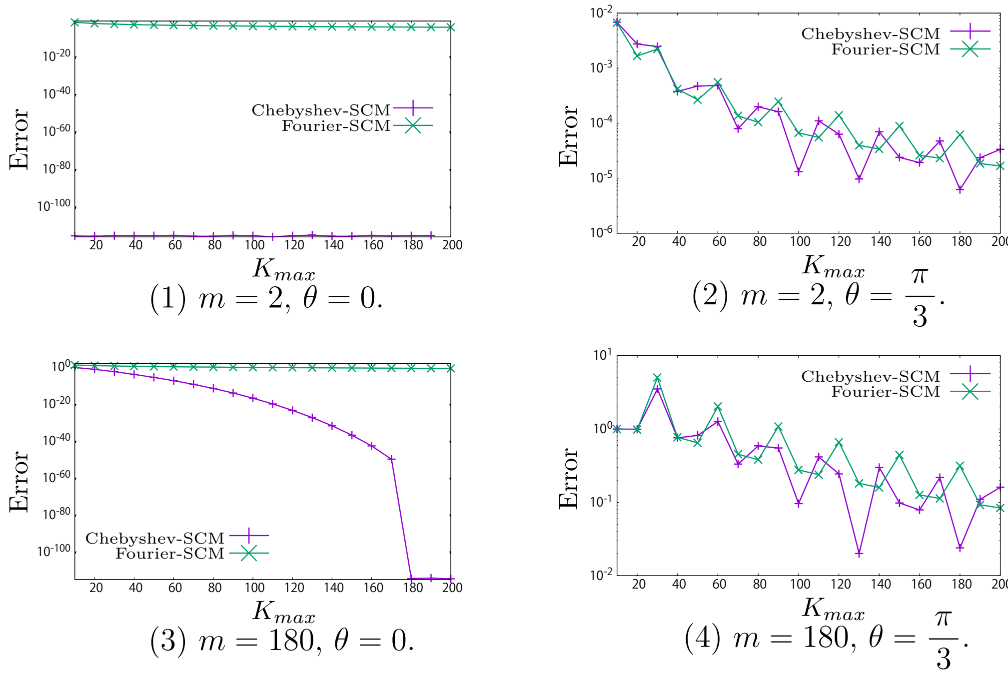

(1) $m = 2$, $\theta = 0$. (2) $m = 2$, $\theta = \dfrac{\pi}{3}$.

(3) $m = 180$, $\theta = 0$. (4) $m = 180$, $\theta = \dfrac{\pi}{3}$.

Figure 5: Error for $F(\theta)$ (power function kernel, $I(\phi) = 1$).

From Figures 4 and 5, it can be seen that Chebyshev-SCM is more accurately superior to Fourier-SCM when the integrand has a sharp peak. However, it must be noted that accuracy of Chebyshev-SCM for $\theta = 0$ and $\theta \neq 0$ is quite different. When accuracy of Chebyshev-SCM is nice (Figures 4(3), 5(1) and 5(3)), unevenly distributed collocation points of Chebyshev-SCM are concentrated near the peak of the integrand. This concentration is useful for capturing the shape of the integrand graph. And this has the effect of improving the approximation of the integrand.

4 PAT(peak adjustment transform)

Here, we consider a transform to concentrate collocation points of Chebyshev-SCM near the peak of the integrand. After that, we propose a variant of the transform for a BVP with RTE.

4.1 Peak adjustment transform

We consider the following tansform;

$$
\begin{aligned}
F(\theta) &\equiv \int_0^{2\pi} p(\phi-\theta)I(\phi)\,d\phi = \int_\theta^{2\pi+\theta} p(\phi-\theta)I(\phi)\,d\phi = \int_0^{2\pi} p(\psi)I(\psi+\theta)\,d\psi \\
&= \int_{-1}^{1} \pi p\left(\pi(z+1)\right) I\left(\pi(z+1)+\theta\right)\,dz.
\end{aligned}
$$

We call this transform PAT(peak adjustment transform). Here, we should remark that Chebyshev-SCM is assumed for the discretization. When we use CGL points, subsequent discretization follows Section 3.2.

$$
Q(z;\theta) \equiv \pi p\left(\pi(z+1)\right) I\left(\pi(z+1)+\theta\right) \fallingdotseq \sum_{k_0=0}^{K_{\max}} Q_{k_0}(\theta) T_{k_0}(z), \tag{10}
$$

$$
Q_{k_0}(\theta) = \frac{2}{K_{\max} c_{k_0}} \sum_{k_1=0}^{K_{\max}} \frac{1}{c_{k_1}} Q(z_{k_1};\theta) T_{k_0}(z_{k_1}), \tag{11}
$$

$$
z_{k_1} = \cos\left(\frac{k_1}{K_{\max}}\pi\right), \quad c_* = \begin{cases} 2, \ * = 0, \ K_{\max}, \\ 1, \ \text{otherwise}, \end{cases} \quad * = k_0, \ k_1. \tag{12}
$$

Thus, our numerical integration by PAT with CGL-SCM is as follows;

$$
F(\theta) = \int_{-1}^{1} Q(z;\theta)\,dz \fallingdotseq \sum_{\substack{k_0=0 \\ k_0\neq 1}}^{K_{\max}} Q_{k_0}(\theta) \frac{1+(-1)^{k_0}}{1-{k_0}^2}. \tag{13}
$$

4.2 Applicable PAT

For the simplicity, we set $K_{\max} = 2K_{half}, \ K_{half} \in \mathbb{Z}_+$. Then, the expression (13) is as follows;

$$
F(\theta) \equiv \int_0^{2\pi} p(\phi-\theta)I(\phi)\,d\phi = \int_{-1}^{1} Q(z;\theta)\,dz \fallingdotseq \sum_{k_0=0}^{K_{half}} Q_{2k_0}(\theta) \frac{2}{1-(2k_0)^2}, \tag{14}
$$

$$
Q_{2k_0}(\theta) = \frac{2}{K_{\max} c_{2k_0}} \sum_{k_1=0}^{K_{\max}} \frac{1}{c_{k_1}} Q(z_{k_1};\theta) T_{2k_0}(z_{k_1}), \quad c_{2k_0} = \begin{cases} 2, \ k_0 = 0, \ K_{half}, \\ 1, \ \text{otherwise}. \end{cases} \tag{15}
$$

In solving problems as a BVP with RTE by SCM, firstly collocation points are set for the solution as follows;

$$I(\phi) = I(\pi(z+1)) \equiv \tilde{I}(z) \fallingdotseq \sum_{k_2=0}^{K_{\max}} I_{k_2} T_{k_2}(z), \tag{16}$$

$$I_{k_2} = \frac{2}{K_{\max} c_{k_2}} \sum_{k_3=0}^{K_{\max}} \frac{1}{c_{k_3}} \tilde{I}(z_{k_3}) T_{k_2}(z_{k_3}) = \frac{2}{K_{\max} c_{k_2}} \sum_{k_3=0}^{K_{\max}} \frac{1}{c_{k_3}} I(\pi(z_{k_3}+1)) T_{k_2}(z_{k_3}), \tag{17}$$

$$z_{k_3} = \cos\left(\frac{k_3}{K_{\max}}\pi\right), \qquad c_{k_3} = \begin{cases} 2, \; k_3 = 0, \; K_{\max}, \\ 1, \; \text{otherwise}. \end{cases} \tag{18}$$

Secondly, we solve discretized equations with $\{I(\pi(z_{k_3}+1))\}$ as unknowns.

Therefore, PAT should be rewritten using $\{I(\pi(z_{k_3}+1))\}$, i.e. as a linear combination of $\{I(\pi(z_{k_3}+1))\}$. For z_{k_1} in (12), we set

$$\psi_{k_1} \equiv \pi(z_{k_1}+1), \qquad \overline{\psi}_{k_1,\theta} \equiv \begin{cases} \psi_{k_1} + \theta, & 0 \le \psi_{k_1} + \theta \le 2\pi, \\ \psi_{k_1} + \theta - 2\pi, & 2\pi < \psi_{k_1} + \theta < 4\pi, \end{cases} \qquad \overline{z}_{k_1,\theta} \equiv \frac{\overline{\psi}_{k_1,\theta}}{\pi} - 1.$$

Then, $0 \le \overline{\psi}_{k_1,\theta} < 2\pi$, $-1 \le \overline{z}_{k_1,\theta} < 1$. From periodicity, $I(\psi_{k_1} + \theta) = I(\overline{\psi}_{k_1,\theta})$. From expressions (16) and (17),

$$\begin{aligned} I(\pi(z_{k_1}+1)+\theta) &= I(\psi_{k_1}+\theta) = I(\overline{\psi}_{k_1,\theta}) \equiv \tilde{I}(\overline{z}_{k_1,\theta}), \\ &\fallingdotseq \sum_{k_2=0}^{K_{\max}} \left(\frac{2}{K_{\max} c_{k_2}} \sum_{k_3=0}^{K_{\max}} \frac{1}{c_{k_3}} I(\pi(z_{k_3}+1)) T_{k_2}(z_{k_3}) \right) T_{k_2}(\overline{z}_{k_1,\theta}). \end{aligned}$$

Therefore, from expressions (14) and (15),

$$\begin{aligned} F(\theta) \fallingdotseq& \sum_{k_0=0}^{K_{half}} \frac{2}{1-(2k_0)^2} \left(\frac{2}{K_{\max} c_{2k_0}} \sum_{k_1=0}^{K_{\max}} \frac{1}{c_{k_1}} \left(\pi\, p(\pi(z_{k_1}+1)) \right.\right. \\ & \left.\left. \left(\sum_{k_2=0}^{K_{\max}} \left(\frac{2}{K_{\max} c_{k_2}} \sum_{k_3=0}^{K_{\max}} \frac{1}{c_{k_3}} I(\pi(z_{k_3}+1)) T_{k_2}(z_{k_3}) \right) T_{k_2}(\overline{z}_{k_1,\theta}) \right) T_{k_0}(z_{k_1}) \right) \right), \\ =& \sum_{k_3=0}^{K_{\max}} \left(\sum_{k_1=0}^{K_{\max}} S_{\theta,k_1,k_3}\, p(\pi(z_{k_1}+1)) \right) I(\pi(z_{k_3}+1)), \end{aligned} \tag{19}$$

where

$$S_{\theta,k_1,k_3} \equiv \frac{4\pi}{(K_{\max})^2 c_{k_1} c_{k_3}} \sum_{k_2=0}^{K_{\max}} \left(\frac{1}{c_{k_2}} T_{k_2}(\overline{z}_{k_1,\theta}) T_{k_2}(z_{k_3}) \left(\sum_{k_0=0}^{K_{half}} \frac{2}{1-(2k_0)^2} \frac{1}{c_{2k_0}} T_{2k_0}(z_{k_1}) \right) \right). \tag{20}$$

PAT used here is called applicable PAT(A-PAT) with CGL-SCM.

Remark.

(i) The right-hand side of (19) is a linear combination of $\{I(\pi(z_{k_3}+1))\}$.

(ii) S_{θ,k_1,k_3} is independent of p and I.

(iii) The computational time of (19) is very much larger than that of (13). However, if S_{θ,k_1,k_3} is prepared in the database, these computational times become almost same.

4.3 Numerical results by PAT

Here, numerical results of A-PAT with CGL-SCM are presented. Since A-PAT and PAT are essentially the same, PAT is used instead of A-PAT in this section. Numerical computations are done in 100 digits using exflib. Here, we should remark that the exact (or theoretical) value must be computed with high accuracy. However, when the kernel is the power function kernel and $I(\phi) \neq 1$, R_m in (7) induces loss of digits. Figure 6 shows this digit loss. Here, the error is defined based on the value computed in 1000 digits. However, 1000 digits computation is costly, So, when the kernel is the power function kernel and $I(\phi) \neq 1$, as the exact value we use 100 digits of the value of P_m or Q_m in (7) computed in 300 digits.

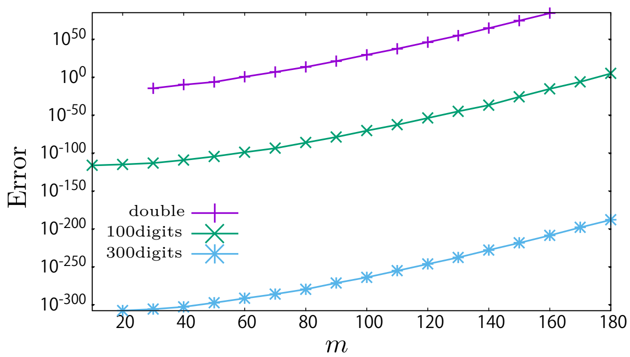

Figure 6: Error for $P_m(0)(I(\phi) = \cos 5\phi)$.

Figures 7 and 8 show numerical results for $I(\phi) = 1$. Error bevhaviors of PAT are independent of θ. This is the result of PAT. When $\theta = 0$, error behaviors of Chebyshev-SCM and PAT are the same as theoretically expected. In Figures 8(2) and 8(4), the accuracy of Fourier-SCM and Chebyshev-SCM is very poor and their two graphs almost coincide. It is shown that PAT attains quite good accuracy when the integrand has a sharp peak. Moreover, Figure 7(2) shows that even if the integrand is gentle, PAT improves the accuracy.

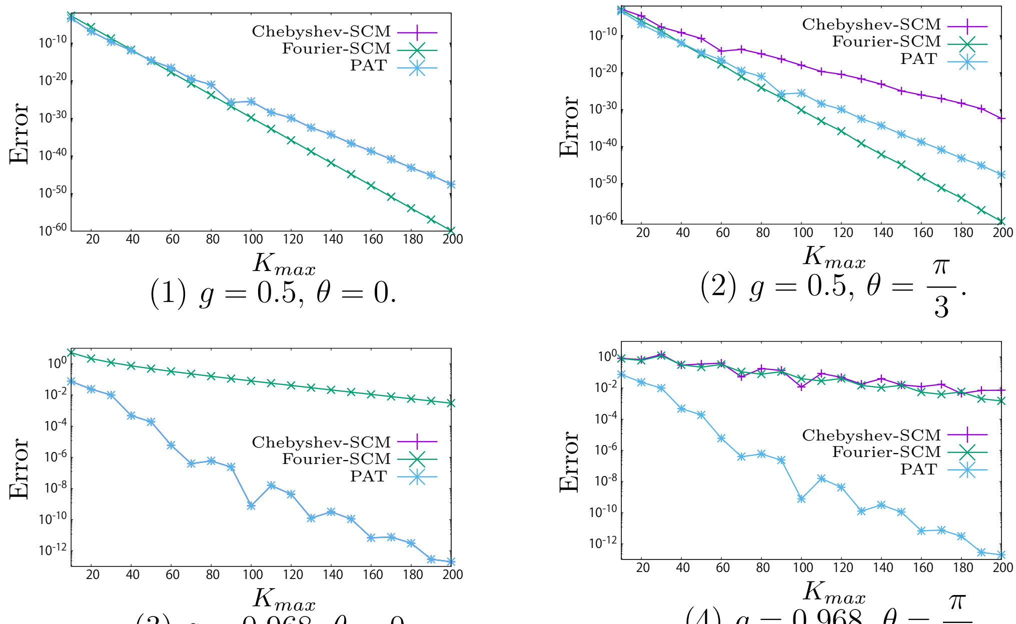

(1) $g = 0.5,\ \theta = 0.$ (2) $g = 0.5,\ \theta = \dfrac{\pi}{3}.$

(3) $g = 0.968,\ \theta = 0.$ (4) $g = 0.968,\ \theta = \dfrac{\pi}{3}.$

Figure 7: Error for $F(\theta)$ by PAT (Poisson kernel, $I(\phi) = 1$).

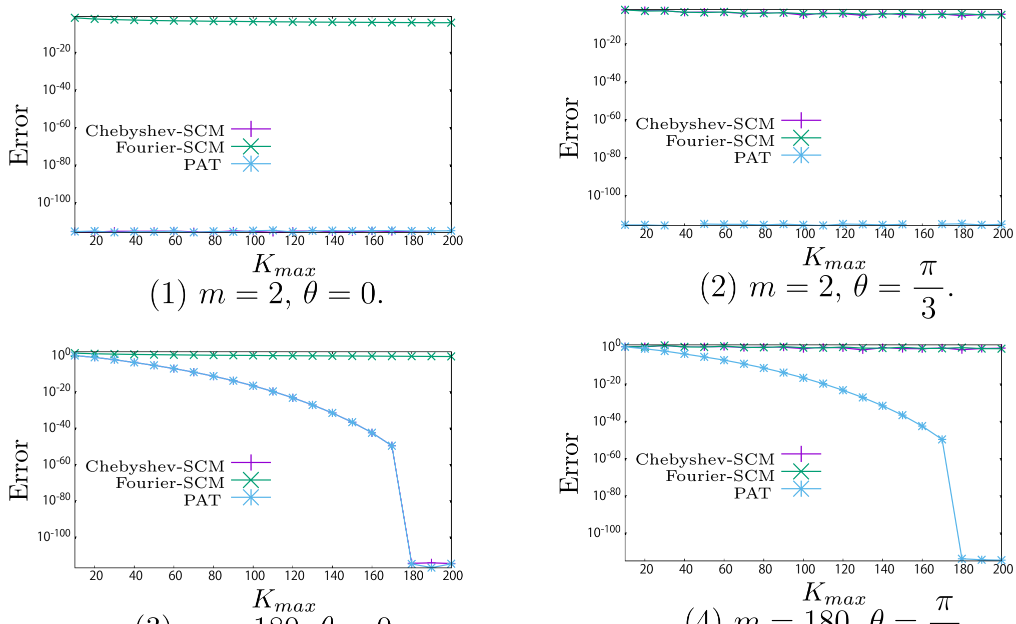

(1) $m = 2,\ \theta = 0.$ (2) $m = 2,\ \theta = \dfrac{\pi}{3}.$

(3) $m = 180,\ \theta = 0.$ (4) $m = 180,\ \theta = \dfrac{\pi}{3}.$

Figure 8: Error for $F(\theta)$ by PAT (power function kernel, $I(\phi) = 1$).

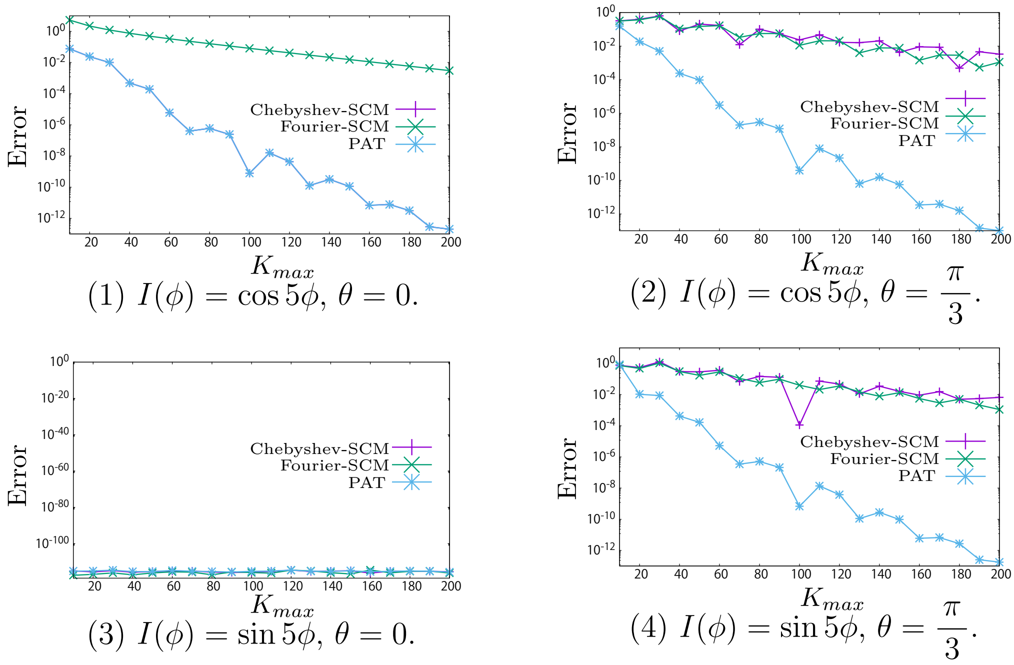

Figure 9: Error for $F(\theta)$ by PAT (Poisson kernel:$g = 0.968$).

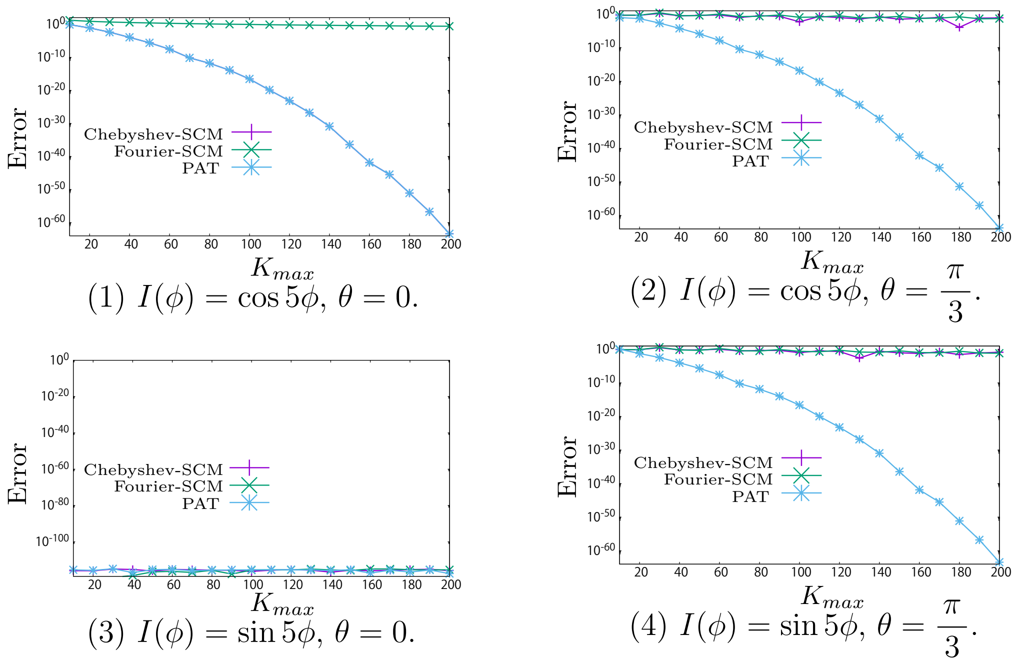

Figure 10: Error for $F(\theta)$ by PAT (power function kernel, $m = 180$).

Figures 9 and 10 show numerical results for $I(\phi) = \cos 5\phi, \sin 5\phi$. As is shown in Figure 3, the graph of the integrand has a sharp peak and it is oscillating, Error bevhaviors of PAT are independent of θ, except for Figures 9(3) and 10(3) where the exact value is 0. In these cases three graphs almost coincide, and there seems to be no truncation error.

This is because the symmetry of the graph of the integrand and the symmetry of the distribution of collocation points match. When $\theta = 0$, error behaviors of Chebyshev-SCM and PAT are the same as theoretically expected. It is shown that PAT attains quite good accuracy.

5 Conclusion

In the paper, we propose a high-precision numerical method for the integration over one period of periodic functions with a sharp peak. The spectral collocation method(SCM) is used for discretization, and numerical computations are performed in multiple-precision. Numerical results by direct applications of Fourier-SCM and Chebyshev-SCM show that the accuracy becomes poor when the peak of the integrand becomes sharp. They also show that the accuracy improves when collocation points of Chebyshev-SCM are concentrated near the peak of the integrand. Therefore, a method called PAT(peak adjustment transform) that concentrates collocation points near the peak is developed. A-PAT(applicable-PAT) which is conscious of general applications is also developed. Numerical results by PAT(A-PAT) are very satisfactory in accuracy.

References

[1] C. Canuto et al., *Spectral Methods: Fundamentals in Single Domains*, Springer-Verlag, Berlin, Heidelberg, 2006.

[2] C. Canuto et al., *Spectral Mthods : Evolution to Complex Geometries and Applications to Fluid Dynamics*, Springer-Verlag, New York, 2007.

[3] K. C. Datta, H. Imai and H. Sakaguchi, On Numerical Challenge for the Distinction Between Smooth Functions and Analytic Functions, Theo. Appl. Mech. Jpn., **62**(2013), pp. 107–117.

[4] H. Fujiwara and Y. Iso, Design of a multiple-precision arithmetic package for a 64-bit computing environment and its application to numerical computation of ill-posed problems, IPSJ J., **44**(3) (2003), pp. 925–931 (in Japanese).

[5] H. Fujiwara, Fast numerical computation for the stationary radiative transport equation using multigrid methods, Trans. JASCOME, **11** (2011), pp. 13–18 (in Japanese).

[6] H. Fujiwara, Numerical challenges to the three dimensional stationary radiative transport equation, Trans. JASCOME, **12** (2012), pp. 43–48 (in Japanese).

[7] H. Fujiwara, Piecewise constant approximation with respect to velocity of the stationary radiative tranport equation, Trans. JASCOME, **16** (2016), pp. 91–96 (in Japanese).

[8] Y. Hoshi and Y. Yamada, Overview of diffuse optical tomography and its clinical applications, J. Biomed. Opt. **21**(9)(2016), 091312.

[9] H. Imai, T. Takeuchi and M. Kushida, On Numerical Simulation of Partial Differential Equations in Infinite Precision, Adv. Math. Sci. Appl., **9**(2) (1999), pp. 1007–1016.

[10] H. Imai, Some Methods for Removing Singularity and Infinity in Numerical Simulation, GAKUTO Internat. Ser. Math. Sci. Appl., **23**(2005), pp. 103–118.

[11] H. Imai and H. Sakaguchi, Numerical Computation on Analyticity of the Solution of a Cauchy Problem for the Backward Heat Equation, Theo. Appl. Mech. Jpn., **56**(2007), pp. 291–300.

[12] A. D. Klose and E. W. Larsen, Light transport in biological tissue based on the simplified spherical harmonics equations, J. Comput. Phys., **220**(2006), pp. 441–470.

[13] H. Soutome and H. Imai, Numerical Regularity Map for Blow-Up Solutions of Nonlinear Ordinary Differential Equations, Adv. Math. Sci. Appl., **29**(2) (2020), pp. 393–402.